

Experimental Characterization of Hydrogen Trapping on API 5CT P110 Steel. Part. I: Effect on Hydrogen Embrittlement Susceptibility

J.A.P. Carrasco^{a*} , J.S. Junior^a, J.M.A. Barbosa^a , E.O. Vilar^c , M.A. dos Santos^b, A.A. Silva^b 

^aUniversidade Federal de Pernambuco, Departamento de Engenharia Mecânica, Recife, PE, Brasil.

^bUniversidade Federal de Campina Grande, Unidade Acadêmica de Engenharia Mecânica, Campina Grande, PB, Brasil.

^cUniversidade Federal de Campina Grande, Unidade Acadêmica de Engenharia Química, Campina Grande, PB, Brasil.

Received: February 02, 2023; Revised: May 15, 2023; Accepted: May 30, 2023

Hydrogen permeation tests and tensile mechanical tests were performed at room temperature on API 5CT P110 steel to characterize hydrogen trapping and to evaluate their hydrogen embrittlement susceptibility. The hydrogen trap density was calculated from two consecutive hydrogen permeation transients plotted using an electrochemical cell. Slow strain rate tensile tests on hydrogen-charged samples through cathodic polarization at different potentials were performed to evaluate the hydrogen embrittlement susceptibility. Thereby it was established the lowest potential that characterizes the onset of the cathodic overprotection for studied steel. After mechanical tests was observed a decrease in ductility as the protection potential became more negative and that the fracture mode was changed from ductile microvoid coalescence on the as-received steel to extended quasi-cleavage on the hydrogen-charged steel. The results showed that API 5CT P110 steel has high susceptibility to hydrogen embrittlement conditioned by a predominance of reversible traps in microstructure and by high hydrogen solubility.

Keywords: *Hydrogen embrittlement susceptibility, hydrogen trapping, hydrogen solubility on steels, API 5CT P110 steel, cathodic overprotection.*

1. Introduction

Corrosion control is of great importance in the offshore oil and gas industry. Cathodic protection is commonly used in subsea pipelines, but its intensive use can lead to so-called cathodic overprotection where large amounts of hydrogen are produced at the coating defects. This hydrogen can be absorbed into the steel and cause hydrogen embrittlement, a degradation process that induces loss of ductility and reduces the fracture resistance of the material¹. The susceptibility of steels to hydrogen embrittlement depends on the diffusivity, solubility, trapping and other hydrogen transport characteristics in the lattice². In turn, trapping depends on microstructural features as grain boundaries, voids, second phase particles and other microstructural heterogeneities, known as hydrogen traps³. Hydrogen traps are classified as reversible and irreversible depending on intensity of their trapping energy⁴. Traps are considered reversible when they possess low trapping energy; as the hydrogen in these traps can be easily released it is considered mobile hydrogen. Traps are considered irreversible when a larger amount of energy must be applied for the hydrogen to be released⁵. When hydrogen is trapped in traps, the diffusion process is altered because the residence time in traps is greater than the residence time in normal interstitial lattice sites; therefore, the main effect of trapping is the reduction of the hydrogen transport rate through the material^{6,7}. At present, it is well established that hydrogen trapping is

a very important part of hydrogen embrittlement⁸ and that the hydrogen embrittlement susceptibility of steel is closely correlated with trapping⁹.

In last years, cracking and failure in subsea and onshore pipelines were partially attributed to embrittlement caused by hydrogen produced from the intensive use of cathodic protection^{10,11}. Although the steels used in pipes for oil and gas transfer and to export petroleum products are characterized by their high mechanical strength and good fracture toughness, these materials are susceptible to some hydrogen damage^{2,12-17}. For this reason, recommended practices^{18,19} and standards²⁰ were prepared for the design of cathodic protection systems in subsea pipelines, taking into account the effects of hydrogen generated in these systems, in order to avoid hydrogen embrittlement processes.

Therefore, the guarantee of the integrity of structures that have cathodic protection systems is necessary in order to sustain the project load capacity. In offshore structures, load capacity is highly important and the constant challenges of the high depths motivate the use of new steel grades, and steels currently used in other applications, in structures with cathodic protection systems. For example, API 5CT P110 steel, which is used in the manufacturing of casing pipes and couplings for oil wells, recently started to be used for the production of tubing and casing for risers, in view of its excellent combination of good fracture toughness and high mechanical strength²¹.

*e-mail: jorge.carrasco@ufpe.br

A preliminary step to evaluate the mechanical response of steels is the study of hydrogen behavior in these materials, in order to obtain the electrochemical parameters required to perform appropriate mechanical tests, or to employ them in mathematical models that allow for numerical simulations with more realistic results, and consequently, with increased accuracy in prediction of failures associated with hydrogen damage²². Trap density also can be obtained experimentally through permeation curves or through mathematical models, either complex or simplified²³, that depend on parameters such as the apparent diffusivity, the effective diffusivity and the subsurface hydrogen concentration. The amount of hydrogen available in the work environment of structures is important information, because this amount will (or will not) enable a sufficient quantity of hydrogen atoms to be absorbed and transported within the lattice to initiate embrittlement processes. In cathodic protection systems, the concentration of hydrogen atoms on the surface of a metal may be orders of magnitude higher than the hydrogen atom concentration created by exposure to hydrogen gas²⁴. In these systems, atomic hydrogen is generated electrochemically in reduction reactions that become more and more dominant as the protection potential takes on more negative values. Therefore, hydrogen availability is strongly associated with the protection potential employed when a cathodic overprotection condition is characterized. According to DNVGL-RPB401¹⁹ the term overprotection is only applicable to protection potentials more negative than -1050 mV, although this is a recommendation of general use. The ISO 15589-2²⁰ standard indicates that for pipeline systems fabricated from steels with $\sigma_y < 550$ MPa, -1100 mV is an adequate negative potential limit. However, for high-strength steels ($\sigma_y \geq 550$ MPa), the most negative potential that can be tolerated without causing hydrogen embrittlement is yet to be determined.

This work studies the hydrogen permeation parameters and hydrogen trapping in API 5CT P110 steel under cathodic overprotection conditions, as well as the resulting changes on its mechanical response to loads and the effect of hydrogen.

2. Method and Experimental Procedures

This study was performed using high strength and low alloy (HSLA) API 5CT P110 steel from a seamless pipe gutter, with intended use in oil well casing, with 330 mm outer diameter and 14 mm wall thickness, provided by CENPES/PETROBRAS.

In order to determine the hydrogen kinetic parameters in the studied steel, potentiodynamic polarization tests were performed to establish the minimum potential for hydrogen generation in the choice electrolyte. With these data, hydrogen permeation tests were performed using Devanathan and Stachurski's²⁵ electrochemical permeation technique. In the permeation tests, first the cathodic protection potential stated by ISO 15589-2 was adopted, then a more negative potential was used in order to ensure cathodic overprotection condition. The saturation times of specimens used in mechanical tensile tests were obtained through the results of permeation tests.

In order to determine variations in ductility and to establish the hydrogen embrittlement susceptibility of studied steel, tensile tests using samples of as-received material and samples of hydrogenated material were performed.

The results of tensile tests were used also to determine the specific range of cathodic protection potentials for the API 5CT P110 steel.

The specimens for all tests were extracted from a pipe wall. The metallic membranes for the electrochemical tests were manufactured with a 3.14 cm² area and 1.0 mm thickness, with their axial direction parallel to rolling direction, according to ASTM G148-97²⁶. The round tensile samples for the mechanical tests were machined in the rolling direction, in accordance to ASTM E8/E8M-09²⁷, with dimensions shown in the schematic of Figure 1.

The Figure 2 shows the Devanathan and Stachurski type electrochemical double-cell²⁵ used in this work for following purposes: (a) obtaining the potentiodynamic curve for choosing the hydrogen production current and (b) testing hydrogen diffusion through the metallic membrane. In the first case, it was only necessary to use one of the cells, forming a classic three-electrode cell. In the second case, the two cells arranged symmetrically were used. The production cell aims to produce hydrogen galvanostatically (or potentiostatically) on the sample surface from the current (or potential) established in the potentiodynamic polarization test. In the detection cell the sample surface is anodically polarized against the potential of the calomel reference electrode (SCE) with the purpose of oxidizing the diffused hydrogen. This oxidation current is recorded continuously to obtain the permeation curve.

The potentiodynamic polarization tests were performed at room temperature ($26 \pm 1^\circ\text{C}$) using the left cell of electrochemical double-cell filled with a NaCl solution, by applying a linear ramp of measured potential against the Ag/AgCl reference electrode at a sweep rate of 0.8 mV/s. A platinum electrode with area of 1 cm² was used as counter electrode in each cell. The concentration and pH of NaCl solution was similar to synthetic seawater solution (24g/l and 8.2 respectively)²⁸. The pH was adjusted with a NaOH solution (0.1N) before starting the tests.

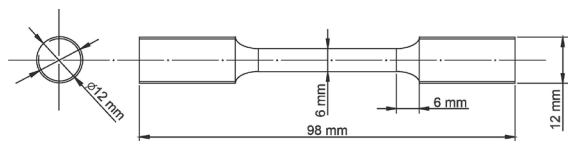


Figure 1. Schematic of round tension test specimen used in tensile tests.

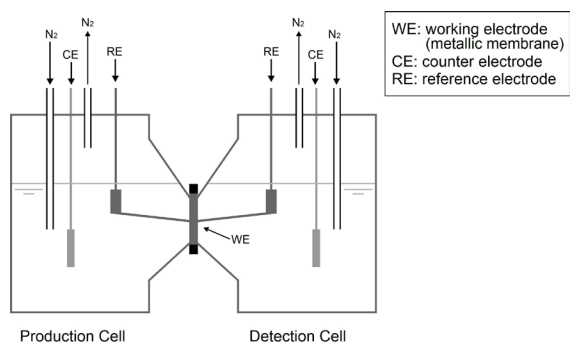


Figure 2. Schematic of electrochemical double-cell used in potentiodynamic polarization and permeation tests²⁵.

The permeation tests were conducted at room temperature ($26 \pm 1^\circ\text{C}$) using metallic membranes placed between the production and detection cells. The galvanostatic method was used to produce hydrogen in the production cell. The choice of the cathodic protection potential followed criteria established by the ISO 15589-2 standard²⁰. The choice of hydrogen production current adopted in each permeation tests were related to the chosen cathodic protection potential and determined from the obtained polarogram in the potentiodynamic test. The production cell was filled with a 24 g/l NaCl solution to avoid the salt deposition or formation of calcareous encrustations that occurs when synthetic seawater is used, since which operate as a barrier to the entry of hydrogen into the material²⁹. The presence of calcareous encrustations decreases the hydrogen flux, making the time for the steady state to be reached during permeation tests longer, but does not affect the diffusivity^{29,30}. For this reason, sodium chloride solutions are very used to replace synthetic seawater in this type of laboratory tests³¹⁻³³. The detection cell was filled with a NaOH solution (0.1N), following the ASTM G148-97²⁶ recommendations. Both solutions were deoxygenated by bubbling N_2 . In the first test, metallic membranes were hydrogen-charged in the production cell through application of a constant reduction current of -3.1 mA, that corresponds to potential of -1100 mV_{Ag/AgCl} according to potentiodynamic polarization curve. This potential was chosen to simulate a cathodic protection condition, although it is suspected that this potential may not be a protection potential for the steel tested. Afterwards, a second test was performed, this time, through application of a constant current of -21 mA, that corresponds to potential of -1300 mV_{Ag/AgCl} according to the same curve, to simulate a cathodic overprotection condition. The detection cell was kept at a constant oxidation potential of +300 mV_{sce}, and the permeated hydrogen was measured by chronoamperometry technique using EC-LAB software (v.10.02) controlled by a Biologic VMP3 multichannel potentiostat. This procedure was repeated two times for each metallic membrane in order to obtain two consecutive hydrogen permeation curves³⁴. Were performed three tests for each condition in order to ensure experimental repeatability.

According to this technique, after the first permeation transient, hydrogen production is interrupted to allow a complete outgassing and a second transient is then obtained after applying a new charge. During the first charge, all traps are filled, and when discharging is performed, only the reversible traps are emptied, for this reason, the second transient should be faster. The difference between the relative positions of transients should reveal the presence and the extent of irreversible trapping.

The steady state hydrogen permeation flux is given by²⁶:

$$J_{ss} = \frac{J_\infty}{F} \quad (1)$$

where J_∞ is the steady state hydrogen permeation current density and F is Faraday's constant. The coefficient of diffusion, D , can be calculated based on the elapsed time (t_{lag}) at $J(t)/J_{ss} = 0.63$ and the breakthrough time (t_b) through the following equations²⁶:

$$D = \frac{L^2}{2t_{lag}} \quad (2)$$

$$D = 0.76 \frac{L^2}{\pi^2 t_b} \quad (3)$$

where L is the membrane thickness. D represents the apparent diffusivity, D_{app} , using the first transients, and the effective diffusivity, D_{eff} , using the second transients. The permeability is given by²⁶:

$$P = J_{ss}L \quad (4)$$

The subsurface hydrogen concentration (solubility) is given by²⁶:

$$C_0 = \frac{J_{ss}L}{D} \quad (5)$$

When $D_L \gg D_{app}$ (D_L is the diffusivity coefficient of pure iron), the trapping density in galvanostatic charging conditions is given by³⁵:

$$N_T = \frac{J_{ss}L}{D_{app}} N_A \quad (6)$$

where N_A is the Avogadro's number.

In tensile mechanical tests several specimens were tested in the as-received condition, and others were tested after being hydrogen-charged. For this reason, before starting mechanical tests one part of round tensile samples of as-received steel was hydrogen-charged in a cathodic protection cell, with schematic shown in Figure 3, filled with synthetic seawater²⁸ without application of mechanical loads. A titanium grid (known as Fischer electrode) surrounding the specimen was used as counter electrode, in order to guarantee the hydrogen flux in all directions.

The hydrogen was produced galvanostatically, and at the same time its cathodic protection potential monitored, during a time enough to get the material to be completely saturated with hydrogen. Characterizing the saturation time is very important, as it may happen that samples charged for very long periods, such as weeks or months, undergo cracking without the application of any external load, giving rise another degradation process.

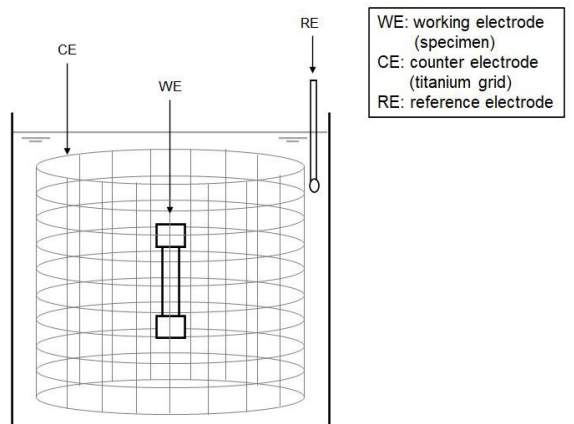


Figure 3. Schematic of cathodic protection cell.

Therefore, saturation times different from those strictly necessary, may mischaracterize the tests. The selected potentials for the hydrogen-charging procedures were: $-1300 \text{ mV}_{\text{Ag/AgCl}}$, $-1100 \text{ mV}_{\text{Ag/AgCl}}$, $-950 \text{ mV}_{\text{Ag/AgCl}}$ and $-900 \text{ mV}_{\text{Ag/AgCl}}$. The saturation times for the potentials of $-1300 \text{ mV}_{\text{Ag/AgCl}}$ and $-1100 \text{ mV}_{\text{Ag/AgCl}}$ were established from results of the first permeation transients, assuming that complete saturation of the material occurs when the steady state is reached. The saturation times for potentials of $-950 \text{ mV}_{\text{Ag/AgCl}}$ and $-900 \text{ mV}_{\text{Ag/AgCl}}$ were estimated since the permeation tests for these potentials were not performed. In this estimation the time calculated for the potential of $-1100 \text{ mV}_{\text{Ag/AgCl}}$ was used as a reference value, understanding that a shorter time than this would be sufficient to saturate a specimen of the same dimensions, with a much lower potential.

The mechanical tensile tests were performed in an INSTRON 5582 universal testing machine. The tensile samples were loaded until fracture at room temperature at a strain rate of $2.5 \cdot 10^{-5} \text{ s}^{-1}$, according to ASTM G129-00³⁶. For the tensile tests on the hydrogenated steel, the hydrogen-charged samples were transferred to testing machine immediately after the completion of the saturation time in the electrochemical cell. The tests were accomplished with a cathodic protection cell coupled to the testing machine, shown in Figure 4, to prevent hydrogen desorption. The potential of $-1300 \text{ mV}_{\text{Ag/AgCl}}$ considered an overprotection potential^{19,20}, was employed in the first test. In the subsequent tests, the “less negative” potentials were employed, until a value was found for which the effect of hydrogen on the mechanical properties of the steel was practically null. The material susceptibility to hydrogen embrittlement was evaluated by determining the embrittlement index, I_{HE} , which compares the ductility of hydrogenated samples (brittle samples) with the ductility of as-received steel samples. Values of this index close to 1 indicate that the material is resistant to hydrogen embrittlement, while lower values indicate a decrease in this resistance and, therefore, an increase in its susceptibility to the degradation process. Very low values indicate that the material is highly susceptible to hydrogen embrittlement. This index is given by³⁶:

$$I_{\text{HE}} = \frac{\epsilon_{\text{H}}}{\epsilon_{\text{f}}} \quad (7)$$

where ϵ_{H} is the failure strain of the hydrogenated samples and ϵ_{f} is the failure strain of the hydrogen-free samples.

Finally, SEM analysis of fracture surface was conducted in order to determine variations in the fracture mode of steel, both without hydrogen and under the effect of hydrogen.

3. Results and Discussion

Figure 5 shows the image of API 5CT P110 steel in the as-received condition captured by an optical microscope.

The microstructural analysis exposes a microstructure composed of fine tempered martensite, typical of quenched and tempered steels, and dispersed carbides. This heat-treatment is required by the API 5CT standard³⁷ for this type of steel. Their chemical composition is shown in Table 1.

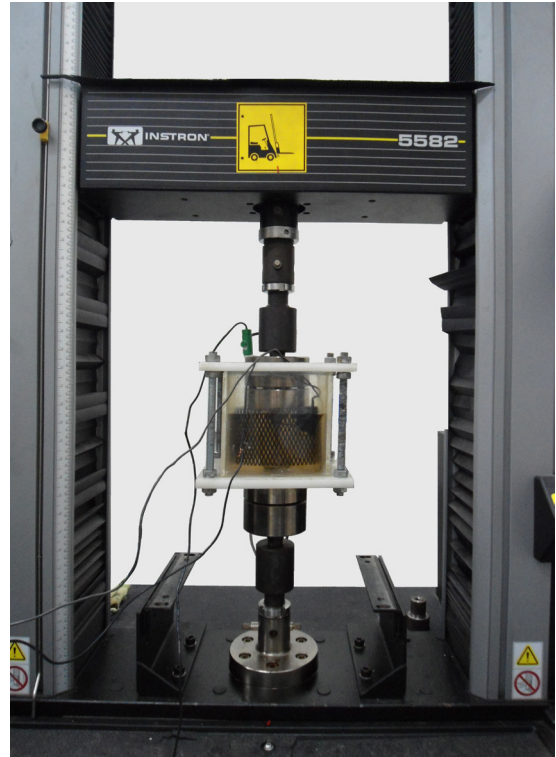


Figure 4. Tensile testing machine with coupled cathodic protection cell.

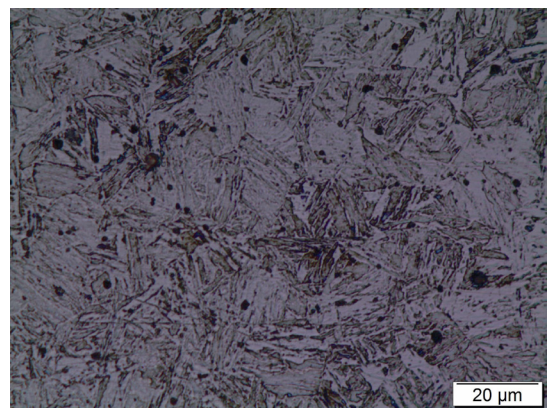


Figure 5. Microstructure of the API 5CT P110 steel in as-received condition (Etchant: Nital 2%. Mag. 1000x).

Table 1. Chemical composition of API 5CT P110 steel (%wt).

C	Si	Mn	P	S	Ni	Cr	Mo	Cu	Al	V	Ti	Fe
0.284	0.242	1.085	0.010	0.006	0.019	0.294	0.136	0.002	0.044	0.006	0.030	Bal

3.1. Electrochemical test

The potentiodynamic polarization curve for API 5CT P110 steel in 24g/l NaCl solution is shown in Figure 6.

The permeation tests were performed under two sets of conditions. In the first test, metallic membranes of as-received steel were hydrogen-charged through application of a constant current of -3.1 mA, that corresponds to potential of -1100 mV_{Ag/AgCl} according to potentiodynamic polarization curve, to simulate a cathodic protection condition²⁰. Afterwards, in a second test was applied a constant current of -21 mA, that corresponds to potential of -1300 mV_{Ag/AgCl} according to potentiodynamic polarization curve, to simulate a cathodic overprotection condition. The hydrogen permeation curves of the as-received steel are shown in Figure 7 and Figure 8. The diffusivity, permeability, and solubility obtained from these curves and the application of Equations 1 to 5, are shown in Table 2.

Table 2 shows that the changes in hydrogen availability related to the two reduction currents, -3.1 mA and -21 mA (which correspond to -1100 mV_{Ag/AgCl}, or cathodic protection condition, and to -1300 mV_{Ag/AgCl}, or cathodic overprotection condition, respectively), affects the hydrogen permeation parameters of steel. This is especially reflected in the decrease of the apparent diffusion coefficient, D_{app} , by a factor of 0.5, and an increase in hydrogen solubility, C_0 , by a factor of 4.8. As the potential becomes more negative, there is a decrease in diffusivity and an increase in solubility, consequently, a greater amount of hydrogen becomes available to migrate towards more attractive regions in lattice. These results show the influence of hydrogen trapping on hydrogen permeation parameters: irreversible traps are quickly saturated with diffusible hydrogen before it is available to fill up the reversible traps and before it continues to diffuse to other locations³⁸. The observed difference in the slopes of the 1st and 2nd transients in Figure 7 and Figure 8 is also a result of hydrogen trapping because it affects the hydrogen elapsed time. According to Van den Eckhout et al.³⁹ reversible trapping has an important influence in the slope of the transients. The greater the reversible trapping, the lower the slope of the curve.

In order to evaluate hydrogen trapping, both transients of each condition must be compared. In Figure 7 and Figure 8, it can be observed that the hydrogen flux in the second transient is smaller, which complicates the evaluation. To overcome this difficulty, curves must be compared in terms of the normalized flux J/J_{ss} and dimensionless time τ ($\tau = \frac{D_{app}t}{L^2}$), according to the procedure proposed by Pressouyre and Bernstein³⁴.

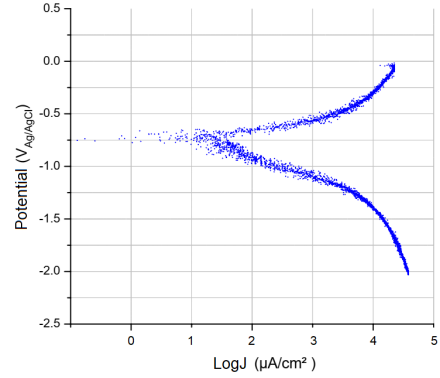


Figure 6. Potentiodynamic polarization curve for API 5CT P110 steel in NaCl solution (24g/l).

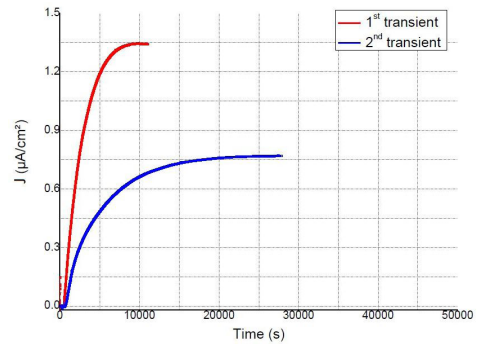


Figure 7. Hydrogen permeation transients of API 5CT P110 steel in NaCl solution (24 g/l) at reduction current of -3.1 mA.

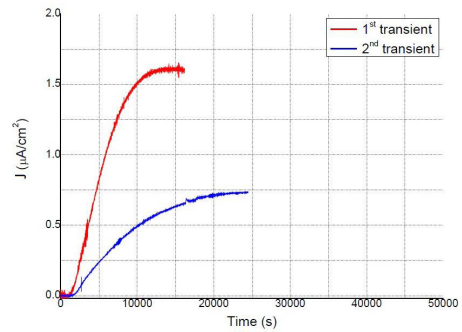


Figure 8. Hydrogen permeation transients of API 5CT P110 steel in NaCl solution (24 g/l) at reduction current of -21 mA.

Table 2. Hydrogen permeation parameters of API 5CT P110 steel.

Current (mA)	Potential (mV _{Ag/AgCl})	Transient	D_{app} (cm ² /s)	D_{eff} (cm ² /s)	P (mol/cm ² ·s)	C_0 (mol/cm ³)
-3.1	-1100	1st	$1.32 \cdot 10^{-6}$		$8.62 \cdot 10^{-13}$	$6.51 \cdot 10^{-7}$
		2nd		$1.65 \cdot 10^{-6}$	$4.87 \cdot 10^{-13}$	$2.95 \cdot 10^{-7}$
-21.0	-1300	1st	$6.55 \cdot 10^{-7}$		$1.61 \cdot 10^{-12}$	$3.15 \cdot 10^{-6}$
		2nd		$1.23 \cdot 10^{-6}$	$3.17 \cdot 10^{-12}$	$2.47 \cdot 10^{-6}$

This procedure assumes that no surface evolution occurs during the entirety of the experimental tests and a steady state is reached. In order to help to better control of the surface phenomena, it is recommended that the exit side of the metallic membrane be covered with a thin palladium layer⁴⁰. In the case of the steel tested in this work, the permeation measurements were conducted without a palladium deposit on the membranes, given that the steady state had been reached in tests.

The extent of reversible trapping is determined by the τ value to which the first transient is displaced. Depending on the reversible trapping density, the second transient is shifted to values closer or further from the first transient; the greater the proximity, the greater the effect of reversible trapping. Therefore, the relative distance between the first and second transients also indicates the irreversible trapping magnitude.

The normalized permeation transients for reductions currents of -3.1 mA and -21 mA (that corresponds to potentials of -1100 mV_{Ag/AgCl} and -1300 mV_{Ag/AgCl} respectively) are shown in Figure 9 and Figure 10. The proximity between the first and the second transients plotted in each of the applied potentials suggest that the extent of irreversible trapping is low for both conditions. For the reduction current of -3.1 mA, the proximity between the two transients and the decrease in the hydrogen breakthrough time indicates that reversible and irreversible trapping both share importance in global trapping. For the reduction current of -21 mA, the proximity between the two transients and the increase in the hydrogen breakthrough time indicates that reversible trapping is the main influence in the overall global trapping. These considerations are closely correlated with the mechanical response of the material to hydrogen effects, which will be discussed later. The global trap density, N_T , the reversible trap density, N_r , and the irreversible trap density, N_i , characterized for each potential obtained from data of these curves, are shown in Table 3.

Table 3 demonstrates that the changes in hydrogen availability related to the two reduction currents, -3.1 mA and -21 mA, affect the hydrogen trapping density of the studied steel. Although alteration in the quantity of reversible and/or irreversible trap sites is not expected, since there are no microstructural changes caused by use of cathodic protection, there is a change in the coverage of these sites due to the greater amount of atomic hydrogen that is solubilized when the current of -3.1 mA (potential of -1100 mV_{Ag/AgCl}) is applied. As solubility increases when the potential for hydrogen generation is more negative, more traps sites are filled. This is reflected by increases in the reversible trapping density, N_r , and to the irreversible trapping density, N_i , by factors of 8.4 and 1.9, respectively.

This indicates that most of the “additional” hydrogen solubilized during the application of the current of -21 mA (potential of -1300 mV_{Ag/AgCl}) is weakly retained in the reversible traps of the microstructure. This fact has important implications in the mechanical response of API 5CT P110 steel under the effect of hydrogen, which will be described below.

The effects of hydrogen on metallic materials have been extensively researched and many works related to the hydrogen trapping have been published⁴¹⁻⁴³. It is now well established that the characteristics of hydrogen traps affect the mechanical behavior of the hydrogenated material, and that the hydrogen susceptibility of steels is closely related to trapping⁴⁴. The hydrogen in irreversible traps has no obvious effect on the fracture behavior of steels⁴⁵. Although some studies show the “beneficial” effect of irreversible trapping^{9,46,47}, others highlight the potential of deep irreversible traps to start cracking when they are saturated with hydrogen^{4,47-49}.

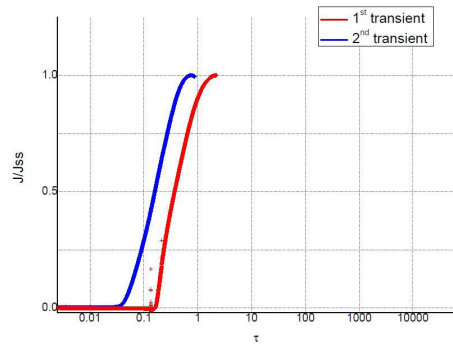


Figure 9. Normalized hydrogen permeation transients of API 5CT P110 steel in NaCl solution (24 g/l) at reduction current of -3.1 mA.

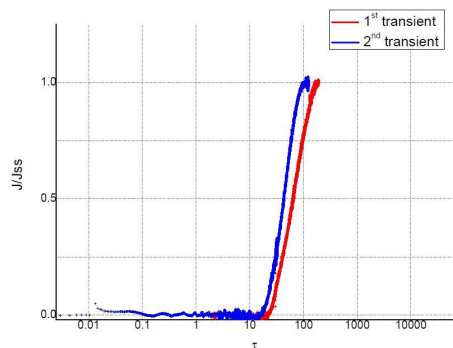


Figure 10. Normalized hydrogen permeation transients of API 5CT P110 steel in NaCl solution (24 g/l) at reduction current of -21 mA.

Table 3. Trapping density of API 5CT P110 steel.

Current (mA)	Potential (mV _{Ag/AgCl})	N_T (sites/cm ³)	N_r (sites/cm ³)	N_i (sites/cm ³)
-3.1	-1100	$3.92 \cdot 10^{17}$	$1.78 \cdot 10^{17}$	$2.14 \cdot 10^{17}$
-21.0	-1300	$1.90 \cdot 10^{18}$	$1.49 \cdot 10^{18}$	$4.08 \cdot 10^{17}$

On the other hand, hydrogen in reversible traps is more harmful because it is able to migrate more easily to the high stress concentration sites, like the crack tips, becoming a fundamental factor for failure to occur^{46,50-52}. Therefore, identifying the dominant trapping type of a steel is crucial for determining its susceptibility to hydrogen embrittlement. In the case of API 5CT P110 was verified that reversible trapping is predominant and, as the hydrogen availability increases, more and more reversible traps are filled. Among other heterogeneities present in the microstructure of studied steel, there are grain boundaries, dislocations (considered reversible traps), Fe_3C and TiC (considered irreversible traps), with activation energy of 20 KJ/mol, 26 KJ/mol, 84 KJ/mol and 95 KJ/mol, respectively^{22,48}.

3.2. Mechanical tests

The tensile mechanical tests were performed on samples of as-received and hydrogen-charged steel, completely saturated. The currents for the selected potentials were obtained through the potentiodynamic polarization curve. The saturation times for the selected cathodic polarization potentials, obtained using the permeation tests results, are shown in Table 4.

The strain-stress curves for samples of the studied steel, without and with hydrogen, are shown in Figure 11. An important loss of ductility can be observed as the applied potential is more negative and the hydrogen production increases. As a large amount of available hydrogen atoms are weakly trapped in the reversible traps and can easily diffuse to stress concentration sites when a mechanical load is applied, hydrogen embrittlement processes can be initiated.

The tensile properties obtained from these curves are shown in Table 5. The embrittlement indices obtained for each test condition show that, in the case of the potential of $-900 \text{ mV}_{\text{Ag}/\text{AgCl}}$ the effect of hydrogen was practically negligible. At the other potentials, this effect becomes increasingly intense as the potentials become more negative.

The main factors that determine the hydrogen embrittlement susceptibility of API 5CT P110 steel are hydrogen solubility and hydrogen trapping ability, conditioned by a predominance of reversible traps in microstructure. Therefore, from the results found here, it can be stated that: a) API 5CT P110 steel is very susceptible to hydrogen embrittlement; b) the cathodic protection potentials in synthetic seawater, for API 5CT P110 steel, are in the range of $-850 \text{ mV}_{\text{Ag}/\text{AgCl}}$ to $-900 \text{ mV}_{\text{Ag}/\text{AgCl}}$ and that more negative potentials can be considered overprotective.

In Table 5 σ_Y is the yield strength, σ_{UTS} is the ultimate tensile strength and ε_f is the failure strain.

3.3. SEM analysis of fracture surface

Figure 12 display SEM images of the fracture surface of the API 5CT P110 steel samples without hydrogen and hydrogen-charged at potentials of $-900 \text{ mV}_{\text{Ag}/\text{AgCl}}$, $-950 \text{ mV}_{\text{Ag}/\text{AgCl}}$ and $-1300 \text{ mV}_{\text{Ag}/\text{AgCl}}$ after the tensile tests.

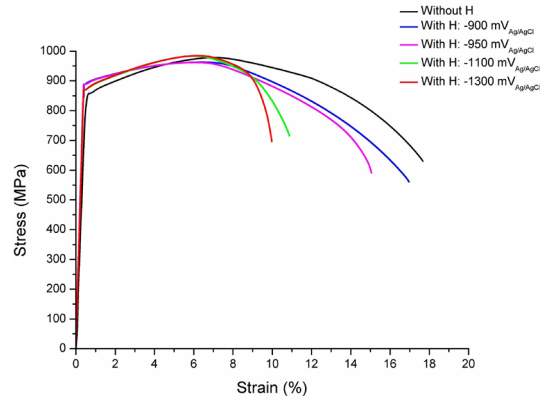


Figure 11. Stress-strain curves of API 5CT P110 steel, without and with hydrogen.

Table 4. Saturation times for tensile specimens under different cathodic polarization potentials.

Potential ($\text{mV}_{\text{Ag}/\text{AgCl}}$)	Current (mA)	Specimen	Diameter (mm)	Saturation time (h)
-900	-0.25	round tensile	6.0	16
-950	-0.31	round tensile	6.0	16
-1100	-3.10	round tensile	6.0	19
-1300	-21.00	round tensile	6.0	38

Table 5. Tensile properties of API 5CT P110 steel, without and with hydrogen.

Parameter	Without hydrogen	With hydrogen			
		Protection Potential ($\text{mV}_{\text{Ag}/\text{AgCl}}$)			
		-900	-950	-1100	-1300
σ_Y (MPa)	856	893	892	874	875
σ_{UTS} (MPa)	978	962	960	981	985
ε_f (%)	16.8	16.6	14.0	10.5	9.9
I_{HE}	---	0.98	0.84	0.62	0.59

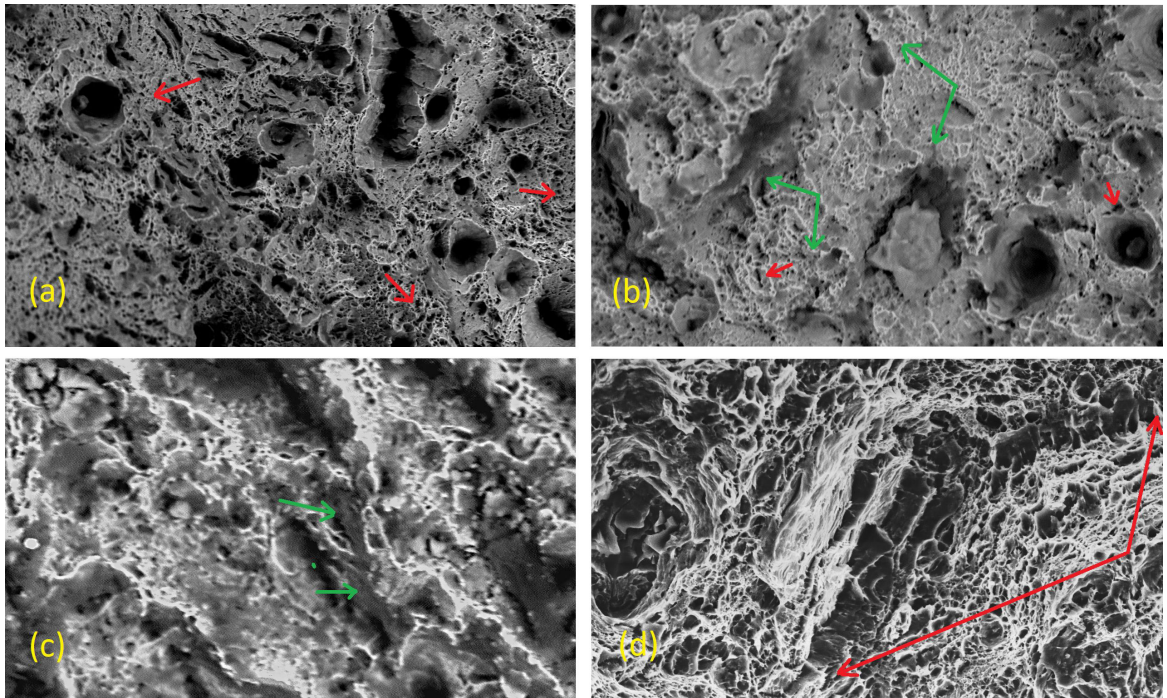


Figure 12. SEM images of fracture surface after tensile tests on samples of API 5CT P110 steel - 2000x: (a) without hydrogen, (b) hydrogen-charged at potential of $-900\text{mV}_{\text{Ag}/\text{AgCl}}$, (c) hydrogen-charged at potential of $-950\text{mV}_{\text{Ag}/\text{AgCl}}$, (d) hydrogen-charged at potential of $-1300\text{mV}_{\text{Ag}/\text{AgCl}}$

The examination of fracture surfaces provides useful information about the role and contribution of hydrogen, generated at different protection potentials, to changes in fracture behavior as well as to the strength and ductility of the steel. In Figure 12(a) dimples (red arrows) can be observed throughout the extent of the fracture surface as result of the microvoids coalescence. This explains the ductile behavior of the metal in as-received conditions.

The causes of the small loss of ductility of hydrogenated steel at the potential of $-900\text{mV}_{\text{Ag}/\text{AgCl}}$ can be identified in Figure 12(b). Microcracks already formed (red arrows) or in a coalescence process for larger cracks (green arrows) can be observed. These cracks are a sign that the steel has undergone localized embrittlement processes, with direct effects on the mechanical response registered by tests. In Figure 12(c), microcracks, dimple rupture and incipient quasi-cleavage regions (green arrows) are observed across the fracture surface. The quasi-cleavage regions and the large number of microcracks explain the more fragile behavior of steel at potential of $-950\text{mV}_{\text{Ag}/\text{AgCl}}$ than at the potential of $-900\text{mV}_{\text{Ag}/\text{AgCl}}$. The fracture surface shown in Figure 11(d) displays large quasi-cleavage regions (red arrows) surrounded by dimple rupture regions. The extension of the quasi-cleavage regions explains the increased steel embrittlement under the potential of $-1300\text{mV}_{\text{Ag}/\text{AgCl}}$.

The changes observed in the fracture surfaces, from ductile microvoid coalescence on the free hydrogen steel to extended quasi-cleavage on the hydrogen-charged steel at potential of $-1300\text{mV}_{\text{Ag}/\text{AgCl}}$, explain the decrease in ductility when protection potential becomes more negative. As quasi-cleavage fracture morphology is characteristic of

hydrogen embrittlement processes⁵³⁻⁵⁵, the increase in the extension of regions showing this fracture mechanism as protection potential becomes more negative indicates that the material is increasingly more brittle as hydrogen generation increases.

The role of hydrogen trapping in the obtained results is crucial. As greater quantity of hydrogen atoms generated at the more negative potentials are weakly trapped in reversible traps, they are able to diffuse to high stress concentration sites, proving the direct relationship between trapping characteristics of API 5CT P110 steel and its high susceptibility to hydrogen embrittlement.

4. Conclusions

In this work the hydrogen trapping in API 5CT P110 steel was characterized experimentally, as well as their hydrogen embrittlement susceptibility was evaluated. The following findings can be drawn from permeation experimental results and from results of tensile mechanical tests:

- i. The API 5CT P110 steel is highly susceptible to hydrogen embrittlement.
- ii. The susceptibility to hydrogen embrittlement of API 5CT P110 steel is strongly associated with the trapping characterized in this research, that is mainly reversible.
- iii. Was observed a decrease in ductility as the protection potential became more negative. The change on fracture mode, from ductile microvoid coalescence on the as-received steel to quasi-cleavage on the hydrogen-charged steel, explain this comportment.

The extension of quasi-cleavage regions is related with degree of material embrittlement.

- iv. The loss of ductility was important for slightly more negative potentials of $-950 \text{ mV}_{\text{Ag/AgCl}}$ and critical to potentials more negative of $-1100 \text{ mV}_{\text{Ag/AgCl}}$. This information should be taken into account in structural integrity assessments of structures made from API 5CT P110 steel that have cathodic protection systems.

Finally, it was established the lowest potential that characterizes the onset of the cathodic overprotection for studied steel, information that can certainly be used for designing cathodic protection systems for underwater structures made of API 5CTP110 steel.

5. Acknowledgments

The authors are very grateful to FINEP/CTPETRO/CNPq/PETROBRAS/RPCMod and to CENPES/PETROBRAS for the technical support, and to LEEq/UAEQ/UFCG and LaMMEA/UAEM/UFCG laboratories for their contribution during the experimental phase.

6. References

1. Ohaeri E, Eduok U, Szpunar J. Hydrogen related degradation in pipeline steel: a review. *Int J Hydrogen Energy*. 2018;43(31):14584-617.
2. Marchetti L, Herms E, Laghoutaris P, Chêne J. Hydrogen embrittlement susceptibility of tempered 9%Cr-1%Mo steel. *Int J Hydrogen Energy*. 2011;36(24):15880-7.
3. Mohtadi-Bonab MA, Masoumi M. Different aspects of hydrogen diffusion behavior in pipeline steel. *J Mater Res Technol*. 2023;24:4762-83.
4. Pressouyre GM. A classification of hydrogen traps in steel. *Metall Trans, A, Phys Metall Mater Sci*. 1979;10(10):1571-3.
5. Oriani RA. The diffusion and trapping of hydrogen in steel. *Acta Metall*. 1970;18(1):147-57.
6. Jemblie L, Olden V, Akselsen OM. A coupled diffusion and cohesive zone modelling approach for numerically assessing hydrogen embrittlement of steel structures. *Int J Hydrogen Energy*. 2017;42(16):11980-95.
7. Castaño Rivera P, Ramunni VP, Bruzzoni P. Hydrogen trapping in an API 5L X60 steel. *Corros Sci*. 2012;54(1):106-18.
8. Taha A, Sofronis P. A micromechanics approach to the study of hydrogen transport and embrittlement. *Eng Fract Mech*. 2001;68(6):803-37.
9. Tsay LW, Chi MY, Wu YF, Wu JK, Lin DY. Hydrogen embrittlement susceptibility and permeability of two ultra-high strength steels. *Corros Sci*. 2006;48(8):1926-38.
10. Shipilov SA, Le May I. Structural integrity of aging buried pipelines having cathodic protection. *Eng Fail Anal*. 2006;13(7):1159-76.
11. Lee C, Jacob R, Morgan P, Weatherhead R. International experiences with cathodic protection of offshore pipelines and flowlines. Stavanger: TWI; 2007.
12. Ananta G, Amarnath N, Nambodhiri TKG. Effect of heat treatments on the hydrogen embrittlement susceptibility of API X-65 grade line-pipe steel. *Bull Mater Sci*. 2003;26(4):435-9.
13. Hardie D, Charles EA, Lopez AH. Hydrogen embrittlement of high strength pipeline steels. *Corros Sci*. 2006;48(12):4378-85.
14. Moro I, Briottet L, Lemoine P, Andrieu E, Blanc C, Odemer G. Hydrogen embrittlement susceptibility of a high strength steel X80. *Mater Sci Eng A*. 2010;527(27-28):7252-60.
15. Chatzidouros EV, Papazoglou VJ, Tsiourva TE, Pantelis DI. Hydrogen effect on fracture toughness of pipeline steel welds, with in situ hydrogen charging. *Int J Hydrogen Energy*. 2011;36(19):12626-43.
16. Zhang L, Shen H, Lu K, Cao W, Sun Y, Fang Y, et al. Investigation of hydrogen concentration and hydrogen damage on API X80 steel surface under cathodic overprotection. *Int J Hydrogen Energy*. 2017;42(50):29888-96.
17. Zhang T, Zhao W, Li T, Zhao Y, Deng Q, Wang Y, et al. Comparison of hydrogen embrittlement susceptibility of three cathodic protected subsea pipeline steels from a point of view of hydrogen permeation. *Corros Sci*. 2017;2018(131):104-15.
18. DNV. DNV-RP-F103: cathodic protection of submarine pipelines. Høvik: DNV; 2019.
19. DNV. DNV-RP-B401: cathodic protection design. Høvik: DNV; 2021.
20. ISO: International Organization for Standardization. ISO 15589-2:2012: Petroleum, petrochemical and natural gas industries — Cathodic protection of pipeline transportation systems — Part 2: Offshore pipelines. Geneva: ISO; 2012.
21. Minerals Manage Systems. Compliant vertical access riser : risk assessment study. Houston: Granherne; 2009.
22. Carrasco JP, Silva Diniz DD, Andrade Barbosa JM, Silva AA, Antonio dos Santos M. Numerical simulation of the hydrogen trapping effect on crack propagation in API 5CT P110 steel under cathodic overprotection. *Int J Hydrogen Energy*. 2019;44(5):3230-9.
23. Araújo DF, Vilar EO, Palma Carrasco J. A critical review of mathematical models used to determine the density of hydrogen trapping sites in steels and alloys. *Int J Hydrogen Energy*. 2014;39(23):12194-200.
24. Ćwiek J. Prevention methods against hydrogen degradation of steel. *J Achiev Mater Manuf Eng*. 2010;43(1):214-21.
25. Devanathan MAV, Stachurski Z. The adsorption and diffusion of electrolytic hydrogen in palladium. *Proc R Soc London Ser A Math Phys Sci*. 1962;270(1340):90-102.
26. ASTM: American Society for Testing and Materials. ASTM G148: standard practice for evaluation of hydrogen uptake, permeation, and transport in metals by an electrochemical technique 1. West Conshohocken: ASTM; 2011.
27. ASTM: American Society for Testing and Materials. ASTM E8/E8M. standard test methods for tension testing of metallic materials 1. West Conshohocken: ASTM; 2010.
28. ASTM: American Society for Testing and Materials. ASTM D1141: standard practice for the preparation of substitute ocean water 1. West Conshohocken: ASTM; 2008.
29. Simoni L, Caselani JQ, Ramos LB, Schroeder RM, Malfatti C F. The influence of calcareous deposits on hydrogen uptake and embrittlement of API 5CT P110 steel. *Corros Sci*. 2017;118:178-89.
30. Hinds G, Turnbull A. Technical note: does calcareous scale formation on cathodically protected steel affect hydrogen uptake? *Corrosion*. 2005;61(9):835-7.
31. Comer A, Looney L. Crack propagation resistance of Zeron 100 GTA and SMA weld metal in synthetic seawater under cathodic overpotential. *Int J Fatigue*. 2008;30(3):444-52.
32. Hörnlund E, Fossen JKT, Hauger S, Haugen C, Havn T, Hemmingsen T. Hydrogen diffusivities and concentrations in 520M carbon steel under cathodic protection in 0.5M NaCl and the effect of added sulphite, dithionite, thiosulphate, and sulphide. *Int J Electrochem Sci*. 2007;2(1):82-92.
33. LaCoursiere MP, Aidun DK, Morrison DJ. Slow strain rate testing for hydrogen embrittlement susceptibility of alloy 718 in substitute ocean water. *J Mater Eng Perform*. 2017;26(5):2337-45.
34. Pressouyre GM, Bernstein IM. A quantitative analysis of hydrogen trapping. *Metall Trans, A, Phys Metall Mater Sci*. 1978;9(11):1571-80.
35. McNabb A, Foster PK. A new analysis of the diffusion of hydrogen in iron and ferritic steels. *Trans Met Soc*. 1963;227:618-27.
36. ASTM: American Society for Testing and Materials. ASTM G129-00: standard practice for slow strain rate testing to evaluate the susceptibility of metallic materials to environmentally assisted cracking 1. West Conshohocken: ASTM; 2006.

37. API: American Petroleum Institute. API 5CT: specification for casing and tubing. 8th ed. Washington, D.C.: API; 2005. ISO: International Organization for Standardization. ISO 11960:2004: petroleum and natural gas industries — steel pipes for use as casing or tubing for wells. Geneva: ISO; 2006.
38. Dadfarnia M, Sofronis P, Neeraj T. Hydrogen interaction with multiple traps: can it be used to mitigate embrittlement? *Int J Hydrogen Energy*. 2011;36(16):10141-8.
39. Van den Eeckhout E, Depover T, Verbeken K. The effect of microstructural characteristics on the hydrogen permeation transient in quenched and tempered martensitic alloys. *Metals (Basel)*. 2018;8(10):779.
40. Manolatos P, Le Coze J, Duret-Thual C, Jérôme M. Use of pure metals to analyse hydrogen electrochemical permeation in steels. *J Phys IV*. 1995;5(7):415.
41. Park GT, Koh SU, Jung HG, Kim KY. Effect of microstructure on the hydrogen trapping efficiency and hydrogen induced cracking of linepipe steel. *Corros Sci*. 2008;50(7):1865-71.
42. Wei FG, Tsuzaki K. Response of hydrogen trapping capability to microstructural change in tempered Fe-0.2C martensite. *Scr Mater*. 2005;52(6):467-72.
43. Huang F, Li XG, Liu J, Qu YM, Jia J, Du CW. Hydrogen-induced cracking susceptibility and hydrogen trapping efficiency of different microstructure X80 pipeline steel. *J Mater Sci*. 2011;46(3):715-22.
44. Brass AM, Guillon F, Vivet S. Quantification of hydrogen diffusion and trapping in 2.25Cr-1Mo and 3Cr-1Mo-V steels with the electrochemical permeation technique and melt extractions. *Metall Mater Trans, A Phys Metall Mater Sci*. 2004;35(5):1449-64.
45. Grabke HJ, Riecke E. Absorption and diffusion of hydrogen in steels. *Mater Tehnol*. 2000;34(6):331-42.
46. Chun YS, Kim JS, Park KT, Lee YK, Lee CS. Role of ϵ martensite in tensile properties and hydrogen degradation of high-Mn steels. *Mater Sci Eng A*. 2012;533:87-95.
47. Tsay LW, Hu YF, Chen C. Embrittlement of T-200 maraging steel in a hydrogen sulfide solution. *Corros Sci*. 2005;47(4):965-76.
48. Maroef I, Olson DL, Eberhart M, Edwards GR. Hydrogen trapping in ferritic steel weld metal. *Int Mater Rev*. 2002;47(4):191-223.
49. Wert CA, Frank RC. Trapping of interstitials in metals. *Annu Rev Mater Sci*. 1983;13:139-72.
50. Depover T, Verbeken K. The detrimental effect of hydrogen at dislocations on the hydrogen embrittlement susceptibility of Fe-C-X alloys: an experimental proof of the HELP mechanism. *Int J Hydrogen Energy*. 2018;43(5):3050-61.
51. Luppò MI, Ovejero-Garcia J. The influence of microstructure on the trapping and diffusion of hydrogen in a low carbon steel. *Corros Sci*. 1991;32(10):1125-36.
52. Scully JR, Dogan H, Li D, Gangloff RP. Controlling hydrogen embrittlement in ultra-high strength steels. Houston: OnePetro; 2004.
53. Martin ML, Fenske JA, Liu GS, Sofronis P, Robertson IM. On the formation and nature of quasi-cleavage fracture surfaces in hydrogen embrittled steels. *Acta Mater*. 2011;59(4):1601-6.
54. Matsumoto Y, Takai K. Method of evaluating delayed fracture susceptibility of tempered martensitic steel showing quasi-cleavage fracture. *Metall Mater Trans, A Phys Metall Mater Sci*. 2017;48(2):666-77.
55. Nagao A, Dadfarnia M, Somerday BP, Sofronis P, Ritchie RO. Hydrogen-enhanced-plasticity mediated decohesion for hydrogen-induced intergranular and “quasi-cleavage” fracture of lath martensitic steels. *J Mech Phys Solids*. 2018;112:403-30.